Local structure modeling of iron doped triglycine sulphate single crystals

M. Bharati[a], V. Singh[a], and R. Kripal[b]

[a]*Department of Physics, Nehru Gram Bharti (DU), Jamunipur, Prayagraj, India.*
[b]*EPR Laboratory, Department of Physics, University of Allahabad, Prayagraj-211002, India.*
Tel: 91-532-2470532; Fax: 91-532-2460993
e-mails: marojbharati99@gmail.com; vikram.singh@ngbu.edu.in; ram_kripal2001@rediffmail.com

Received 13 February 2024; accepted 4 August 2024

Zero field splitting parameters of iron doped triglycine sulphate single crystals are evaluated with the help of superposition model and the perturbation theory. These parameters are in reasonable agreement with the experimental values taking local distortion into account. The theoretical result supports the experimental observation that iron occupies interstitial position in triglycine sulphate crystal. Using crystal field analysis program with crystal field parameters from superposition model as input, the optical spectra of the system are computed. A reasonable match between the computed and experimental energy values is obtained. Thus the theoretical investigation supports the experimental conclusion. The present modeling approach may be useful in other ion-host systems to explore crystals for technological and industrial applications.

Keywords: Organic compounds; single crystal; crystal fields; electron paramagnetic resonance; zero field splitting.

DOI: https://doi.org/10.31349/RevMexFis.71.010501

1. Introduction

Electron paramagnetic resonance (EPR) provides local site symmetry and zero field splitting (ZFS) parameters of transition ions in crystals [1,2]. The theoretical determinations of zero-field splittings for $3d^5$ ions are difficult due to zero orbital angular momentum in the $^6\mathbf{S}$ ground state [3,4]. Two theoretical methods; first, the microscopic mechanism and the second, the superposition model, are generally used to find zero-field splittings for $3d^5$ ions in crystals [5,6]. For the first method, out of many mechanisms contributing to zero-field splitting, the spin-orbit coupling mechanism is important as the contributions from other mechanisms are negligible [7-10]. Hence, the calculated values based on the spin-orbit coupling mechanism come out to be in reasonable agreement with the observed values [7-10]. The same mechanism is applied here.

Triglycine sulphate, $[NH_2CH_2(CH_3COOH)_3.H_2SO_4]$ (TGS) is a pyroelectric type ferroelectric crystal which allows their use as photodetector element in infrared spectroscopy and night vision applications. TGS detectors have also been used as the target in vidicon cathode ray imager tubes [11,12]. Fe^{3+} doped TGS are used in constructing bi-stable ferroelectric memory and quantum state capacitors [13]. TGS crystals doped with different paramagnetic ions have been studied earlier [14-17]. The temperature range of EPR measurements of the iron-doped TGS crystal is extended to find a possibility of different iron co-ordinations and the dynamics of iron-glycine complexes [18]. In TGS: Fe^{3+} crystal Fe^{3+} ions occupy interstitial positions. The Fe^{3+} ion is surrounded by two glycine molecules (GII and GIII) and two SO_4 groups [18]. In this crystal with a higher iron concentration, the EPR spectrum is not observed at room temperature. It is due to the broadening of the EPR line above 200 K because of the thermal motion of ligands. As the temperature is reduced, the amplitude of the thermal motion of ligands decreases, and the EPR line narrows. At 100 K, two new orientations of paramagnetic complexes A and B appear in the spectrum. The ZFS parameters D and E obtained for Fe^{3+} in TGS crystal having higher iron concentration at 4.2 K for non-equivalent complexes A and B are of the same order [18]. The g tensor components from the powder spectrum suggest small rhombic distortion. Hence, the complexes A and B have distorted octahedral co-ordination. In addition to A and B, there is EPR spectrum due to another non-equivalent complex C in this crystal. The complex C is characterized by the ZFS parameter quite larger than that of the complexes A and B [18]. This implies that the relaxation time T_1 for this complex is probably shorter than for complexes A and B. Therefore, the co-ordination of the Fe^{3+} ion is perhaps different in complex C. Mossbauer study of Fe^{3+} doped TGS crystal [19] has shown that in addition to complexes of octahedral co-ordination there are possibilities to have complexes of tetrahedral co-ordination. This provides a larger D value resulting from a shortened metal-ligand distance.

In the present investigation, the ZFS parameters D and E are calculated for the Fe^{3+} ion at interstitial sites A, B and C using CF parameters and perturbation equations [20]. The purpose is to find the location of Fe^{3+} ion and the distortion occurred in the crystal. The results obtained for the Fe^{3+} ions at interstitial sites in TGS crystal with local distortion provide reasonable match with the experimental values. The present process may be used to various other ion-host systems to explore crystals for technological and industrial applications.

2. Crystal structure

Ferroelectric TGS has monoclinic structure [21] at room temperature with lattice parameters $a = 9.417$ Å, $b = 12.643$ Å, $c = 5.735$ Å, $\beta = 110'23'$, the space group is $P2_1$, and the polar direction is along the two-fold screw axis. Out of the three glycine molecules in the crystal, one has the usual zwitter-ion cofiguration, the remaining two glycines are mono-protonated and planar. They are designated as glycinium ions [21].

The crystal structure of TGS with symmetry adopted axis system (SAAS) is shown in Fig. 1. The location of Fe^{3+} ion is also shown.

3. Calculations of crystal field and zero field splitting parameters

The following spin Hamiltonian [22,23] is used to analyze the EPR spectrum,

$$\mathscr{H} = \left(\mu_B B.g.S + D\left\{S_Z^2 - \frac{1}{3}S(S+1)\right\} + E(S_x^2 - S_y^2)\right), \quad (1)$$

where g, μ_B, B, D and E are the spectroscopic splitting factor, Bohr magneton, external magnetic field, second rank axial and rhombic ZFS parameters, respectively [24-26]. The laboratory axes (x, y, z) are parallel to the modified crystallographic axes a, b, $c*$. The symmetry adopted axes (SAA) (local site symmetry axes) are the mutually perpendicular directions of metal-ligand bonds. The Z-axis of SAAS is along the crystal c*-axis and the rest two axes (X, Y) are in the ab plane as shown in Fig. 1. When Fe^{3+} ion are doped in TGS crystal, these occupy interstitial sites with some distortion [27].

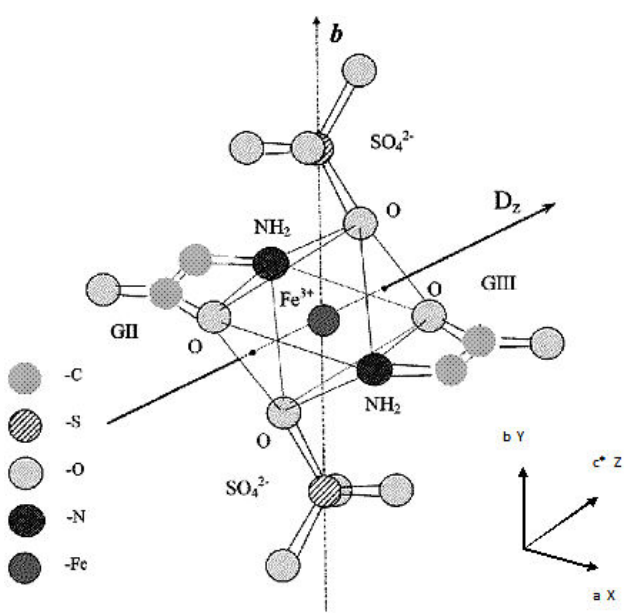

FIGURE 1. Crystal structure of triglycine sulphate with symmetry adopted axis system (SAAS). The location of Fe^{3+} ion is also shown.

The spin Hamiltonian of a $3d^5$ ion is given as [28,29],

$$\mathscr{H} = \mathscr{H}_o + \mathscr{H}_{so} + \mathscr{H}_{ss} + \mathscr{H}_c, \quad (2)$$

$$\mathscr{H}_c = \sum B_{\mathrm{kq}} C_q^{(k)}, \quad (3)$$

where B_{kq} are the CF parameters in Wybourne notation and $C_q^{(k)}$ are the Wybourne spherical tensor operators. In the crystal field of orthorhombic symmetry, $B_{\mathrm{kq}} \neq 0$ only for $k = 2, 4$; $q = 0, 2, 4$. The CF parameters, B_{kq} are calculated using SPM [28,30-33].

In TGS crystal the local field symmetry around Fe^{3+} ions is taken to be orthorhombic (OR-I) [27] and in this symmetry, the ZFS parameters D and E are obtained as [33]:

$$D = \left(\frac{3\varsigma^2}{70P^2D}\right)[-B_{20}^2 - 21\varsigma B_{20} + 2B_{22}^2] + \left(\frac{\varsigma^2}{63P^2G}\right)[-5B_{40}^2 - 4B_{42}^2 + 14B_{44}^2], \quad (4)$$

$$E = \left(\frac{\sqrt{6}\varsigma^2}{70P^2D}\right)[2B_{20} - 21\varsigma]B_{22} + \left(\frac{\varsigma^2}{63P^2G}\right)[3\sqrt{10}B_{40} + 2\sqrt{7}B_{44}]B_{42}, \quad (5)$$

where $P = 7B+7C$, $G = 10B+5C$, $D = 17B+5C$, B and C are Racah parameters and ς is the spin-orbit coupling parameter. Using average covalency parameter N, $B = N^4B_0$, $C = N^4C_0$, $\varsigma = N^2\varsigma_0$, where B_0 and C_0 are Racah parameters for free ion and ς_0 is the free ion spin-orbit coupling parameter [28,34]. For free Fe^{3+} ion, $B_0 = 1130$ cm^{-1}, $C_0 = 4111$ cm^{-1} and $\varsigma_0 = 589$ cm^{-1} [28].

The average parameter N is determined from $N = (\sqrt{B/B_0} + \sqrt{C/C_0})/2$ with the help of Racah parameters ($B = 610$ cm^{-1}, $C = 2360$ cm^{-1}) evaluated from optical study of the Fe^{3+} ion in Ni L-Histidine Hydrochloride Monohydrate Crystals with similar ligands [35].

The CF parameters, in terms of co-ordination factor $K_{\mathrm{kq}}(\theta_j, \varphi_j)$ and intrinsic parameter $\overline{A_\kappa}(R_j)$, using SPM are given [33,36] as

$$B_{\mathrm{kq}} = \sum_j^{\overline{A_k}} (R_j) K_{\mathrm{kq}}(\theta_j, \varphi_j). \quad (6)$$

The intrinsic parameter $\overline{A_\kappa}(R_j)$ is obtained as

$$\overline{A_k}(R_j) = \overline{A_k}(R_0)\left(\frac{R_0}{R_j}\right)^{t_k}, \quad (7)$$

where R_j is the distance of the d_n ion from the ligand, $\overline{A_k}(R_0)$ is the intrinsic parameter of the reference crystal, R_0 is the reference distance between the metal and ligand ion and t_k is the power law exponent.

TABLE IA. Atomic coordinates in triglycine sulphate single crystal (sites A and B) along with spherical polar coordinates (without and with distortion) (R, θ, φ).

Position of Fe^{3+}	Ligands	Spherical polar coordinates of ligands					
		x	y	z	R(nm)	θ^0	φ°
			(Å)				
			Without distortion				
Site: Interstitial	O(II)	0.2218	0.4975	0.7646	0.3434 R_1	85.68 θ_1	94.66 φ_1
Fe (0.5003,	O'(II)	0.4596	0.5397	0.7988	0.1894 R_2	81.11 θ_2	91.24 φ_2
0.5065,	N(II)	0.0939	0.5800	0.3063	0.3710 R_3	93.08 θ_3	96.29 φ_3
0.5061)	O(III)	0.7824	0.4931	0.2229	0.3567 R_4	94.55 θ_4	85.45 φ_4
	O'(III)	0.5454	0.4825	0.2317	0.1793 R_5	98.80 θ_5	88.54 φ_5
	N(III)	0 9068	0.4331	0.7059	0.3711 R_6	86.91 θ_6	83.70 φ_6
			Without distortion				
A			O(II)			$0.5034R_1 + \Delta R_1$	
			O'(II)			$0.4194R_2 + \Delta R_2$	
			N(II)			$0.5810R_3 + \Delta R_3$	
			O(III)			$0.5767R_4 + \Delta R_4$	
			O'(III)			$0.1820R_5 + \Delta R_5$	
			N(III)			$0.5511R_6 + \Delta R_6$	
			Without distortion				
B			O(II)			$0.4334R_1 + \Delta R_1$	
			O'(II)			$0.3454R_2 + \Delta R_2$	
			N(II)			$0.4690R_3 + \Delta R_3$	
			O(III)			$0.5767R_4 + \Delta R_4$	
			O'(III)			$0.1793R_5 + \Delta R_5$	
			N(III)			$0.5511R_6 + \Delta R_6$	

TABLE IB. Atomic coordinates in triglycine sulphate single crystal (site C) along with spherical polar coordinates (without and with distortion) (R, θ, φ).

Position of Fe^{3+}	Ligands	Spherical polar coordinates of ligands					
		x	y	z	R(nm)	θ^0	φ°
			(Å)				
			Without distortion				
Site: Interstitial	O(II)	0.2218	0.4975	0.7646	0.3434 R_1	85.68 θ_1	94.66 φ_1
Fe (0.5003,	N(II)	0.0939	0.5800	0.3063	0.3710 R_2	93.08 θ_2	96.29 φ_2
0.5065,	O(III)	0.7824	0.4931	0.2229	0.3567 R_3	94.55 θ_3	85.45 φ_3
0.5061)	N(III)	0 9068	0.4331	0.7059	0.3711 R_4	86.91 θ_4	83.70 φ_4
			Without distortion				
C			O(II)			$0.2334R_1 + \Delta R_1$	
			N(II)			$0.2610R_2 + \Delta R_2$	
			O(III)			$0.2607R_3 + \Delta R_3$	
			N(III)			$0.2731R_4 + \Delta R_4$	

The crystal-field parameters B_{kq} are obtained using Eq. (6) as follows:

$$B_{20} = \overline{A_2}(R_0)[(R_0/R_1)^{t_2}(3\cos^2\theta_1 - 1) + (R_0/R_1^{'})^{t_2}(3\cos^2\theta_1^{'} - 1) + (R_0/R_2)^{t_2}(3\cos^2\theta_2 - 1) + (R_0/R_2^{'})^{t_2}(3\cos^2\theta_2^{'} - 1)], \quad (8)$$

$$B_{22} = \sqrt{6}\overline{A_2}(R_0)[(R_0/R_1)^{t_2}\sin^2\theta_1 + (R_0/R_1^{'})^{t_2}\sin^2\theta_1^{'} - (R_0/R_2)^{t_2}\sin^2\theta_2 - (R_0/R_2^{'})^{t_2}\sin^2\theta_2^{'}]/2, \quad (9)$$

$$B_{40} = \overline{A_4}(R_0)[(R_0/R_1)^{t_4}(35\cos^4\theta_1 - 30\cos^2\theta_1 + 3) + (R_0/R_1^{'})^{t_4}(35\cos^4\theta_1^{'} - 30\cos^2\theta_1^{'} + 3) + (R_0/R_2)^{t_4}(35\cos^4\theta_2 - 30\cos^2\theta_2 + 3) + (R_0/R_2^{'})^{t_4}(35\cos^4\theta_2^{'} - 30\cos^2\theta_2^{'} + 3)], \quad (10)$$

$$B_{42} = \sqrt{10}\overline{A_4}(R_0)[(R_0/R_1)^{t_4}\sin^2\theta_1(7\cos^2\theta_1 - 1) + (R_0/R_1^{'})^{t_4}\sin^2\theta_1^{'}(7\cos^2\theta_1 - 1) - (R_0/R_2)^{t_4}\sin^2\theta_2(7cos^2\theta_2 - 1) - (R_0/R_2^{'})^{t_4}\sin^2\theta_2^{'}(7\cos^2\theta_2^{'} - 1)], \quad (11)$$

$$B_{44} = \sqrt{70}\overline{A_4}(R_0)[(R_0/R_1)^{t_4}\sin^4\theta_1 + (R_0/R_1^{'})^{t_4}\sin^4\theta_1^{'} + (R_0/R_2)^{t_4}\sin^4\theta_2 + (R_0/R_2^{'})^{t_4}\sin^4\theta_2^{'}]/2. \quad (12)$$

For Fe^{3+}doped crystals, $t_2 = 3$ and $t_4 = 5$ are used [32]. The same values are considered in the above calculation. As the co-ordination around Fe^{3+} ion is octahedral for A and B sites, $\overline{A_4}$ is found from the relation [37] $\overline{A_4}(R_0) = (3/4)\ D_q$. Using optical study [35], the value of $D_q = 700$ cm^{-1}. Hence, the value of $\overline{A_4}\,(R_0) = 525$ cm^{-1}. For 3d^5 ions the ratio $\overline{A_2}/\overline{A_4}$ lies between 8 to 12 [28,38,39]. Taking, $\overline{A_2}/\overline{A_4} = 10$ gives $\overline{A_2} = 5250$ cm^{-1}. For interstitial site C the coordination of Fe^{3+} ion is tetrahedral and so $\overline{A_4}(R_0) = -27/16$ D_q is taken [37]. The D_q value in this case is obtained as in [40] based on the number of ligands (NL). Taking 700 cm^{-1} for NL = 6 as in Fe^{3+} doped Ni L-Histidine Hydrochloride Monohydrate (NiLHH) [35] and then multiplying this D_q by the respective ratio 4/6. This yields $Dq = 467$ cm^{-1} and hence, the value of $\overline{A_4}\,(R_0) = 788.1$ cm^{-1}. Using $\overline{A_2}/\overline{A_4} = 10$ gives $\overline{A_2} = 7881$ cm^{-1} for site C.

4. Results and discussion

The CF parameters $B_{\rm kq}$ of Fe^{3+} ion at interstitial sites are determined using SPM and parameters $\overline{A_2}$ and $\overline{A_4}$ with arrangement of ligands about Fe^{3+} ion as shown in Fig. 1. Atomic coordinates in TGS single crystal along with spherical polar coordinates (without and with distortion) (R, θ, φ) for sites A, B and C are given in Table IA, IB. The CF parameters $B_{\rm kq}$ employing Eqs. (8-12) and transformation S2 for standardization [26] and ZFS parameters D and E together with reference distance R_0 are shown in Table II. Table II shows that the value of $R_0 = 0.200$ nm slightly less than the sum of ionic radii of Fe^{3+} = 0.0645 nm and $O^{2-} = 0.184$ nm along with local distortion yield ZFS parameters for interstitial octahedral sites A and B in reasonable agreement with the experimental values [18]. The ZFS parameters found using $R_0 = 0.200$ nm and without local distortion are larger than

TABLE II. Crystal field parameters B_{kq} and zero field splitting parameters D, E of iron doped triglycine sulphate single crystal for sites A, B and C (without and with distortion).

		Crystal- field parameters (cm^{-1})					Zero-field splitting parameters ($\times 10^{-4}$ cm^{-1})		
Site	R_0 (nm)	B_{20}	B_{22}	B_{40}	B_{42}	B_{44}	|D|	|E|	|E|/|D|
				Without distortion					
Site A and B	0.200	-16066.2	-20399.7	4006.726	4441.273	8714.667	15351.0	7296.0	0.475
				Without distortion					
Site A	0.200	-9106.81	6896.817	2015.322	2241.123	5491.739	4074.0	1170.0	0.287
							Exp. 4070.0	330.0	0.081
Site B	0.200	-10342.9	7847.965	2248.124	2498.268	5874.428	4882.0	1463.0	0.299
							Exp. 4880.0	380.0	0.078
				Without distortion					
Site C	0.200	-5337.8	-6479.11	480.8945	158.9685	3473.989	2224.0	1002.0	0.450
				Without distortion					
Site C	0.200	-16538.6	13339.89	6236.146	2059.895	9395.735	11638.0	3862.0	0.330
							Exp. 11630.0	400.0	0.081

TABLE III. Experimental and calculated energy band positions of iron doped triglycine sulphate single crystal for sites A, B and C (octahedral and tetrahedral)

Transition from $^6A_{1g}$(S)	Observed wave number (cm^{-1})			Calculated wave number (cm^{-1})					
	NiLHH:Fe^{3+}	YAG:Fe^{3+}		A		B		C	
$^4T_{1g}$(G)	13789	$^4T_{1g}$(G)	15700	14055	14083	13024	14903	16308	16443
				15418	15490	14984	15465	16502	16659
				16259	16400	15585	16682	16687	17151
$^4T_{2g}$(G)	17236	$^4T_2$(G)	19000	17239	17368	16940	17376	18248	19582
				17423	17511	17384	18028	19611	19684
				17859	17883	18104	18342	19716	19873
		$^4A_1$(G)						21023	21037
^4E_g(G)		^4E(G)	21190	21117	21313	21241	21284	21101	21122
				21355	22249	22219	22336	21634	22227
$^4T_{2g}$(D)		$^4T_2$(D)	24210	25152	25424	24755	25193	24069	24167
				25793	25907	25580	26174	24448	24632
				25986	26076	26296	26553	25301	26006
^4E_g(D)		^4E(D)	26600	27235	27498	27090	27246	26470	26965
				27537	27576	27696	27868	27223	27297
$^4T_{1g}$(P)		$^4T_1$(P)	27320	29961	30033	30631	30929	27902	28227
				30264	30777	31066	31115	29049	29288
				31127	31155	31368	31448	29384	29594

the experimental values. For interstitial site C considering $t_2 = 3$ and $t_4 = 5$ yield E/D larger than 0.33, the standard value [26]; therefore $t_2 = 3$ and $t_4 = 1.5$ with transformation S2 have been used to obtain E/D ratio 0.33. From Table II, it is seen that the ZFS parameters D and E thus obtained for site C are in reasonable match with the experimental values. The ZFS parameters found for site C using $R_0 = 0.200$ nm and without local distortion are quite different from the experimental values.

Using B_{kq} parameters (with distortion) and CFA program [41,42] the optical spectra of Fe^{3+} doped TGS single crystals are calculated. The energy levels of the Fe^{3+} ion are found after diagonalization of the complete Hamiltonian. The calculated and experimental [35,43] energy values are shown in Table III for all interstitial sites A, B and C (octahedral and tetrahedral). The experimental energy values for tetrahedral coordination of Fe^{3+} ion are taken from Fe^{3+} doped yttrium aluminium garnet(YAG: Fe^{3+}) having similar ligands [43]. From Table III, a reasonable match between the calculated and experimental energy values is found. Thus, the theoretical analysis employing SPM supports the experimental result that Fe^{3+} ions occupy interstitial sites in the TGS single crystal with octahedral and tetrahedral coordinations [18].

5. Conclusions

Zero field splitting parameters for Fe^{3+} ions doped TGS single crystals have been evaluated using superposition model and perturbation theory. The calculated zero field splitting parameters show reasonable agreement with the experimental ones. The calculated optical band positions also give reasonable agreement with the experimental values. Thus, the theoretical result found on the basis of superposition model supports the experimental one that Fe^{3+} ions occupy interstitial sites in TGS single crystal. The present modeling approach may be useful in other ion-host systems to explore crystals for technological and industrial applications.

Acknowledgement

The authors are thankful to the Head, Department of Physics, University of Allahabad, Allahabad for providing departmental facilities and to Prof. C. Rudowicz, Faculty of Chemistry, Adam Mickiewicz University, Poznan, Poland for providing CFA program.

Declarations

Ethical approval

This research did not contain any studies involving animal or human participants, nor did it take place on any private or protected areas. No specific permissions were required for corresponding locations.

Competing interests:

The authors declare that they have no known competing financial interests or personal relationships that could have appeared to influence the work reported in this paper.

Authors contributions

Maroj Bharati and Vikram Singh- performed calculations, wrote the manuscript and prepared the figure.
Ram Kripal- idea and supervision.
All authors have reviewed the manuscript.

Funding

No funding is received.

Availability of data and materials

The data will be made available on request.

1. F. E. Mabbs, D. Collison and D. Gatteschi, Electron Paramagnetic Resonance of d Transition Metal Compounds; (Elsevier, Amsterdam, 1992).
2. J. A. Weil and J. R. Bolton, Electron Paramagnetic Resonance: Elementary Theory and Practical Applications; 2nd ed., (Wiley, New York, 2007).
3. D. J. Newman, On the g-shift of S-state ions. *J. Phys. C: Solid State Phys.* **10** (1977) L315, https://doi.org/10.1088/0022-3719/10/11/008.
4. E. Siegel, K. A. Muller, Local position of Fe^{3+} in ferroelectric $BaTiO_3$. *Phys. Rev. B*, **20** (1979) 3587, https://doi.org/10.1103/PhysRevB.20.3587.
5. Y. Y. Yeung, Local distortion and zero-field splittings of $3d^5$ ions in oxide crystals. *J. Phys. C: Solid State Phys.* **21** (1988) 2453, https://doi.org/10.1088/0022-3719/21/13/010.
6. T. H. Yeom, S. H. Choh, M. L. Du, A theoretical investigation of the zero-field splitting parameters for an Mn^{2+} centre in a $BiVO_4$ single crystal. *J. Phys.: Condens. Matter* **5** (1993) 2017, https://doi.org/10.1088/0953-8984/5/13/017.
7. R. R. Sharma, Spin-Lattice Coupling Constants of an Fe^{3+} Ion in MgO, *Phys. Rev.* **176** (1968) 467, https://doi.org/10.1103/PhysRev.176.467.
8. R. R. Sharma, Zero-Field Splitting of a ^6S Ion in Trigonal Symmetry, *Phys. Rev. B* **3** (1971) 76, https://doi.org/10.1103/PhysRevB.3.76.
9. W. L. Yu, Cubic zero-field splitting of a ^6S state ion. *Phys. Rev. B*, **39** (1989) 622, https://doi.org/10.1103/PhysRevB.39.622.
10. W. C. Zheng, S. Y. Wu, Theoretical investigations of the temperature dependence of zero-field splitting for in crystals, *J. Phys.: Condms. Mutter.* **9** (1997) 5081, https://doi.org/10.1088/0953-8984/9/24/008.
11. B. Subramanian, H. C. Zeng, Water-assisted reconstruction on ferroelectric domain ends of triglycine sulfate $(NH_2CH_2COOH)_3$Â·H_2SO_4 crystals, *J. Mater. Chem.* **10** (2000) 651, https://doi.org/10.1039/A907937H.
12. M. D. Aggarwal *et al.*, Pyroelectric materials for uncooled infrared detectors : processing, properties, and applications. National Aeronautics and Space Administration, Marshall Space Flight Center. OCLC 754804811 (2010).
13. A. Nautiyal, T C Upadhyay, Theory of Iron Doped Deuterated Triglycine Sulphate Doped Ttriglycine Sulphate (Fe-DTGS) Crystal, *Int. J. Chem. Sci. Appl.*, **4** (2013) 29.
14. J. Stankowski, Molecular dynamics of ferroelectric crystals of the triglycine sulphate family, *Phys. Rep.* **77** (1981) 1, https://doi.org/10.1016/0370-1573(81)90005-3.
15. J. Stankowski, A. Wieckowski, S. Hedewy, Second-Order Effects and Hyperfine Structure of Nitrogen and Hydrogen in the EPR Spectrum of Glycine Chelate with $^{63}Cu^{2+}$ in Triglycine Sulphate, *J. Magn. Reson.* **15** (1974) 498, https://doi.org/10.1016/0022-2364(74)90151-6.
16. A. K. Abass, F. Y. M. Al-Eithan, Absorption Edge Measurements of Ttriglycime Sulfate Single Crystal Doped with-Chromium, *J. Phys. Chem. Solids* **47** (1986) 933, https://doi.org/10.1016/0022-3697(86)90104-6.
17. W. Windsch, G. Volkel, Electron Paramagnetic Resonance Investigations of Cr3 Doped Ferroelectric Triglycine Sulphate Monocrystals: Part 1: Structural Change During Phase Transition, *Ferroelectrics* **9** (1975) 187, https://doi.org/10.1080/00150197508237722.
18. Sz. Los, Z. Trybula, EPR Study of Fe^{3+} Paramagnetic Centers in Doped Triglycine Sulphate Crystals, *Acta Phys. Polon. A* **101** (2002) 279, https://doi.org/10.12693/aphyspola.101.279.
19. I. E. G. Morrison, L. V. C. Rees, J. Silver, E. A. D. White, Mössbauer investigation of iron-doped triglycine sulphate, *J. Chem. Soc. Dalton Trans*. (1976) 1103, https://doi.org/10.1039/DT9760001103.
20. W. L. Yu, M.G. Zhao, Spin-Hamiltonian parameters of ^6S state ions. *Phys. Rev. B* **37** (1988) 9254, https://doi.org/10.1103/PhysRevB.37.9254.
21. S. Hoshino, Y. Okaya, R. Pepinsky, Crystal Structure of the Ferroelectric Phase of $(Glycine)_3$Â·H_2SO_4, *Phys. Rev.* **115** (1959) 323, https://doi.org/10.1103/PhysRev.115.323.
22. A. Abragam, B. Bleaney, Electron Paramagnetic Resonance of Transition Ions; (Clarendon Press, Oxford, 1970).
23. C. Rudowicz, Concept of spin Hamiltonian, forms of zero field splitting and electronic Zeeman Hamiltonians and relations between parameters used in EPR. A critical review. *Magn. Reson. Rev.* **13** (1987) 1.
24. C. Rudowicz and H. W. F. Sung, Can the electron magnetic resonance (EMR) techniques measure the crystal (ligand) field

parameters?. *Physica B: Cond. Matt.* **300** (2001) 1, https://doi.org/10.1016/S0921-4526(01)00568-3.

25. C. J. Radnell, J. R. Pilbrow, S. Subramanian, M. T. Rogers, Electron paramagnetic resonance of Fe^{3+} ions in $(NH_4)_2SbF_5$. *J. Chem. Phys.* **62** (1975) 4948, https://doi.org/10.1063/1.430410.
26. C. Rudowicz, R. Bramley, On standardization of the spin Hamiltonian and the ligand field Hamiltonian for orthorhombic symmetry. *J. Chem. Phys.* **83** (1985) 5192, https://doi.org/10.1063/1.449731.
27. B. N. Figgis, M. A. Hitchman, Ligand Field Theory and its Applications; (Wiley, New York, 2000).
28. T. H. Yeom, S. H. Choh, M. L. Du, M. S. Jang, EPR study of Fe^{3+} impurities in crystalline $BiVO_4$. *Phys. Rev. B* **53** (1996) 3415, https://doi.org/10.1103/PhysRevB.53.3415.
29. C. Rudowicz, S. K. Misra, Spin-Hamiltonian formalisms in electron magnetic resonance (EMR) and related spectroscopies. *Appl. Spectrosc. Rev.* **36** (2001) 11, https://doi.org/10.1081/ASR-100103089.
30. Z. Y. Yang, C. Rudowicz, Y. Y. Yeung, Microscopic spin-Hamiltonian parameters and crystal field energy levels for the low C_3 symmetry Ni^{2+} centre in $LiNbO_3$ crystals. *Physica B: Cond. Matt.* **348** (2004) 151, https://doi.org/10.1016/j.physb.2003.11.085.
31. Z. Y. Yang, Y. Hao, C. Rudowicz, Y. Y. Yeung, Theoretical investigations of the microscopic spin Hamiltonian parameters including the spin-spin and spin-other-orbit interactions for Ni^{2+} ($3d^8$) ions in trigonal crystal fields. *J. Phys.: Condens. Matter* **16** (2004) 3481, https://doi.org/10.1088/0953-8984/16/20/018.
32. T. H. Yeom, Y. M. Chang, S. H. Choh, C. Rudowicz, Experimental and Theoretical Investigation of Spin-Hamiltonian Parameters for the Low Symmetry Fe^{3+} Centre in $LiNbO_3$. *Phys. Stat. Sol. b* **185** (1994) 409, https://doi.org/10.1002/pssb.2221850211.
33. C. Rudowicz, Z. Y. Yang, Y. W. Lun, Crystal field analysis for $3d^4$ and $3d^6$ ions with an orbital singlet ground state at orthorhombic and tetragonal symmetry sites, *J. Phys. Chem. Solids* **53** (1992) 1227, https://doi.org/10.1016/0022-3697(92)90043-D.
34. C. K. Jorgensen, Modern Aspects of Ligand Field Theory; (North-Holland, Amsterdam, 1971), p.305.
35. V. Parvathi, J. Sai Chandra, Y.Sunandamma, Growth, Characterization and NLO activity of Fe (III) doped Ni L-Histidine Hydrochloride Monohydrate Crystals, IOSR *Journal of Engineering*, **4** 92014043-4050.
36. D. J. Newman, B. Ng, The superposition model of crystal fields. *Rep. Prog. Phys.* **52** (1989) 699-763.
37. D. J. Newman, B. Ng (Eds.), Crystal Field Handbook; (Cambridge University Press, Cambridge, 2000).
38. D. J. Newman, D. C. Pryce, W. A. Runciman, Superposition model analysis of the near infrared spectrum of Fe (super 2+) in pyrope-almandine garnets. *Am. Miner.* **63** (1978) 1278-1281.
39. A. Edgar, Electron paramagnetic resonance studies of divalent cobalt ions in some chloride salts. *J. Phys. C: Solid State Phys.* **9** (1976) 4303, https://doi.org/10.1088/0022-3719/9/23/015.
40. S. Pandey, R. Kripal, A. K. Yadav a, M. Açıkgöoz, P. Gnutek, C. Rudowicz, Implications of direct conversions of crystal field parameters into zero-field splitting ones-Case study: Superposition model analysis for Cr^{3+} ions at orthorhombic sites in $LiKSO_4$, *J. Lumin.* **230** (2021) 117548, https://doi.org/10.1016/j.jlumin.2020.117548.
41. P. Gnutek, Z. Y Yang, C. Rudowicz, Modeling local structure using crystal field and spin Hamiltonian parameters: the tetragonal FeK_k^{3+}-O_I^{2-} defect center in $KTaO_3$ crystal. *J. Phys.: Condens. Matter* **21** (2009) 455402 (11pp). https://doi.org/10.1088/0953-8984/21/45/455402.
42. Y. Y. Yeung, C. Rudowicz, Crystal Field Energy Levels and State Vectors for the 3dN Ions at Orthorhombic or Higher Symmetry Sites. *J. Comput. Phys.* **109** (1993) 150, https://doi.org/10.1006/jcph.1993.1206.
43. Y. SugitaniI, K. Tagawa, K. Kato, Optical absorption spectra of iron (III) and chromium (III) doped in synthetic yttrium-aluminium-garnets (YAG), *Miner. J.* **7** (1974) 445, https://doi.org/10.2465/minerj1953.7.445.